Research Article

Spatial Dynamics of Indoor Radio Wideband Channels

Dana Porrat,[1] Aawatif Hayar,[2] and Yuval Serfaty[1]

[1] *School of Computer Science and Engineering of the Hebrew University of Jerusalem, Jerusalem 91904, Israel*
[2] *EURECOM, Route des Crêtes, BP: 193 06560 Sophia Antipolis France, France*

Correspondence should be addressed to Dana Porrat, dana.porrat@huji.ac.il

The multipath components of superwideband (2–17.2 GHz) nonline-of-sight channel responses measured inside several buildings are stable along sections that are 27 cm long on average with a standard deviation of 16 cm. The stability regions of multipath components have an approximately log-normal histogram. An analysis of measured channels that explicitly includes finite spatial areas of visibility of the multipath components is superior to the classic analysis that attributes spatial dynamics to interference of the multipath. The spatial stability of measured responses, that is, the size of the typical area of visibility of each multipath component, decreases as the carrier frequency increases but does not depend on bandwidth. The results offer insight into the nature of the diffuse part of the radio channel.

1. Introduction

The temporal dynamics of radio channels are intimately related to their variation in space. Temporal channel variation is usually attributed either to movement of the terminals, as in the case of a mobile telephone held while walking, or movement of objects in the environment of the communications system.

The analysis of measured or simulated wideband channels is normally carried out in the time domain, that is, in the form of impulse responses. The angle of arrival of each multipath component, together with the motion of the receiving antenna, determines the shift in path arrival time as the receiver moves. The Doppler shift of a multipath component is a frequency-domain concept; it is manifested in the impulse response by a location-dependent time of arrival of the multipath components. The spread of Doppler shifts of the different components that constitute a whole channel response is often thought to be the main cause of channel variation in space or time.

The classical description of channel dynamics in time is the coherence period that characterizes the typical period where the channel tends to be more or less constant. In the classic channel model, the coherence period is inversely related to the Doppler spread of the response. Channel analysis that is based on the Doppler spread implicitly assumes that each, multipath component is received over the entire region of receiver locations [1]. We test this assumption using a large measurement campaign to find that it is not realistic even for decimeter scale regions.

The common view of multipath channels assumes that spatial dynamics are caused by the interference of multipath components. We tested this assumption by comparing two reconstructions of measured impulse responses based on extracted multipath components; in the "unbounded" reconstruction each component was present along the entire (one-meter) range of receiver locations, and in the "bounded" reconstruction they had finite areas of visibility. The results indicate that interference of stable multipath components gives a significantly inferior reconstruction of the channel when compared with a reconstruction that attributes to each path a limited area of visibility.

The results show a clear decrease, in the average and in the standard deviation of the length of the visibility area, as the carrier frequency increases in the range from 2 GHz to 17 GHz. We conclude that the channel is spatially more stable at lower bands. The apparent stability of the multipath components is unaffected by variation of the bandwidth between 100 MHz and 1.5 GHz.

A possible explanation follows the idea of "wideband Fresnel zones" suggested in [2–5]. In particular, in [5] a Fresnel zone analysis that predicts effective areas of scattering off objects that decrease in size as the carrier frequency increases is suggested. The reduction in the effective area

of scattering causes a reduction in the range of receiver locations where each multipath component is apparent.

Channel stability has significant implications on various aspects of system design. In particular, multiple antenna (MIMO) systems benefit from small-scale channel variation over space, because variations in the channel mean that the different links (between one transmiting antenna and one receiving antenna) are uncorrelated even if the antennas at each terminal are close to each other.

Our analysis shows average multipath component visibility lengths on the order of a few decimeters. Results from [6] measured correlation lengths of 5–15 cm; other related work has concentrated on the correlation of path amplitudes [7, 8] as they vary along space and on the predictability of path amplitude values [9]. Our work is unique as it focuses on the existence of individual paths in adjacent areas in space. Instead of assuming that paths are stable and investigating the evolution of their amplitudes in space, we analyze the appearance of paths as the receiver moves.

Recent MIMO channel models that rely on indoor channel measurements include the spatial dynamics of multipath clusters via birth and death processes. A model based on measurements with a bandwidth of 80 MHz [10] is presented in [11] this bandwidth does not allow inspection of the dynamics of individual multipath components. Another MIMO model that includes cluster birth and death dynamics is presented in [12]. The measurements used to validate this model were taken with a bandwidth of 200 MHz.

Most models of radio channels, that is, the 3GPP Spatial Channel Model [13], IEEE 802.11n [14], and the WINNER model [15–17], do not include the effects of movement of the terminals in space. The models describe the spatial dependence of the channel via angles of departure and angles of arrival of the propagating waves from the transmitter and to the receiver. The spatial dynamic aspect is sometimes described via correlations or coherence distances of various channel parameters.

The COST 259 model [18, 19] describes "visibility regions" for clusters of multipath components in macrocell (outdoor) environments. The model indicates the probability distribution function of the location of the visibility regions. A separate set of visibility regions is randomly generated for each cluster.

For picocell (indoor) environments the COST 259 model describes the birth and death of multipath components using the Poisson process following the work of Zwick and collaborators [20]. The spatial dynamics of indoor radio channels were measured with a 120 MHz bandwidth and modelled by Chong et al. [21, 22] and Herdin [23], and with a 30 MHz bandwidth by Nielsen et al. [24]. Spatial dynamics due to blocking of the LoS by people are discussed in [25], and spatial variations of shadowing are shown in indoor-outdoor channels in [26].

2. Measurement Environment and Equipment

2.1. The System. The measurement setup was based on an Agilent N5230 network analyzer, connected to two omni-directional antennas (Electro-Metrics EM-6865) in the 1–18 GHz band with suitable amplifiers. The receiving antenna was placed on a meter long linear motorized positioner with submillimeter accuracy that was moved between measurements but was kept immobile during the collection of each channel response. The transmitting antenna was placed on a cart that was moved to different locations for different measurements but was immobile during each measurement. Measurements were normally performed during nights, when movement of people around the system was minimal. One antenna was characterized in an anechoic chamber to verify its response.

Calibration was performed using measured responses of the cables and amplifiers that is, their responses were removed from the channel responses used for analysis. The (mild) frequency-dependent responses of the antennas were also removed, but we could not compensate for the slight deviation of the antenna patterns from the nominal omni-directional pattern. We also did not attempt to compensate for the vertical pattern of the antennas.

We tested the effect of the metallic receiver cart in two ways: (1) by comparing measurements with the cart covered with absorbing material to measurements taken with the cart exposed and (2) by comparing measurements with the cart direction reversed (rotated by 180°). No significant effects were seen.

2.2. The Measurement Environment. The 50 measurements used in this paper were collected between 2006 and 2008 in four office buildings in the Givat Ram campus of the Hebrew University in Jerusalem and in the Holon Institute of Technology; these buildings have a standard cement and cement block construction. We kept the equipment in a single floor of each building in most of the measurements, and separated them to adjacent floors in five measurements. Transmitter-receiver separation ranged from 2 to 30 meters. All measurements were non-line-of-sight (NLoS).

3. Analysis

The analysis is based on estimating the individual multipath components, and it focuses on their spatial area of visibility. A *measurement* in this work is a collection of responses measured with a stationary transmitter and a receiver located at positions that were uniformly spread over a one-meter rail in steps of 2 to 10 mm. The receiver was held stationary during the measurement of each impulse response.

We analyze the measured channel responses using a raised cosine window with 3 dB points at 2 GHz and 17.2 GHz and $\beta = 0.1$ for the full-band results (Section 4.1) and 3 dB bands of 1 GHz in Section 4.2. After filtering, the measured responses were converted to the time (delay) domain with a 28 psec time step, to generate a two-dimensional real representation of the channel as shown in the example in Figure 1. The channel measurement matrix **M** has rows that span a single channel impulse response the columns span receiver positions. The delay range was set at 150 nsec around the maximal (absolute) response at one end
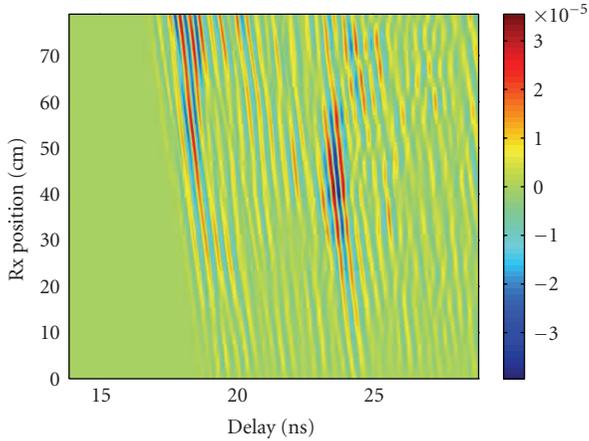
FIGURE 1: An example of measured impulse responses. The horizontal axis has delay and vertical receiver positions. The responses are real with amplitudes that are shown in color. This measurement was taken with terminal separation of 9.8 m and is typical of near line-of-sight situations. The color reflects linear amplitude values that may be negative.

of the rail; this seemed sufficient to include all the significant parts of the response.

The temporal resolution of 28 psec was maintained in all our analyses that is, responses with bandwidths of 1 GHz are heavily oversampled. Due to the oversampling, apparent multipath components with similar delays are correlated.

All the measurements included in this analysis were of sufficient SNR, that is, at least dB, and most cases above 20 dB (42 out of 50). To calculate the SNR we used the maximum (absolute) amplitude among the multipath components, and normalized its square by the noise variance, calculated from a late 5 nsec section of the response over all the available receiver positions.

A significant feature of our measurements is the finite, and usually short, spatial extent of the multipath components. Figure 1 is typical in this sense, this feature can be seen also in channel responses presented in [27]. The diagonals extend 10–60 cm over receiver positions in Figure 1. Line of sight (LoS) measurements have more stable direct components that extend beyond the one meter measured length.

Our analysis is based on a software tool designed to extract the multipath components from the measurements. This tool received measured impulse responses of the type shown in Figure 1 and returned a list of diagonals, each defined by its endpoints its width and a constant real (possibly negative) amplitude. A brief overview of multipath extraction tools follows and then a description of our multipath extraction tool.

3.1. Wideband Multipath Extraction.

The CLEAN algorithm was introduced from radio astronomy into the analysis of UWB measured channels by *Cramer* [28] and coauthors [29, 30]. CLEAN is essentially an iterative search for the strongest multipath component in channel responses from

a single transmitter measured at an array of receivers. The algorithm receives (temporal) impulse responses as input it searches over delay and angles of arrival and iteratively removes the strongest MPC from the measurement data until the remaining data is weak enough.0020Liu et al. [31] suggest a modification that accounts for distortion, based on the usage of multiple templates of the received pulse shape.

The SAGE (Space-Alternating Generalized Expectation-maximization) algorithm was introduced for radio channel analysis by Fleury et al. [32, 33] for the extraction of delay and angle of arrival from narrowband and wideband signals. The extension to UWB and the addition of successive cancellation into SAGE were suggested by Chong et al. (FD-SAGE) [34] and Haneda & Takada (UWB-SAGE) [35]. The FD-SAGE algorithm was further enhanced in [36] from SIMO to MIMO settings.

RIMAX [37] is an algorithm similar to SAGE in the fact it iterates over the MPC parameters RIMAX is based on an improved gradient-based parameter estimation that operates simultaneously over the entire set of parameters. It iterates between the specular and the diffuse components of the channel.

An extension RIMAX that is based on an extended Kalman Filter was suggested in [38]. The Kalman Filter utilizes a state-space approach on top of RIMAX and tracks parameters over successive measurement locations. The introduction of the state-space approach made it possible to derive parameters faster than conventional high-resolution algorithms (including RIMAX) since the parameter estimates at one terminal location were used as the initial values for estimates at adjacent terminal locations. This approach extracts long MPCs sustained over a sufficiently large area of terminal locations and attributes other parts of the channel response to the diffuse component.

A high-resolution algorithm of this family for ultrawideband signals was presented in [39], and a path tracking mechanism was introduced in [40], that says that "significant paths constantly exist in many (terminal) positions" and attempts to estimate only such MPCs.

The method used in the current work is based on a non-parametric search for energetic sections in the two-dimensional (spatial-temporal) channel response matrix. No assumptions are made on the channel model, and only two threshold parameters are used.

Santos, Karedal et al. [41, 42] recently presented a frequency-based algorithm that searches over reflector positions and uses successive cancellation it is different from CLEAN and SAGE in two significant points: (1) each MPC may be received at delays that can vary nonlinearly over a linearly spaced receiver array and (2) each MPC may be received over part of the receiver array.

Our method is similar to that of Santos et al. in that it allows MPCs that impinge over parts of the receiver array. The significant new feature is the millimetric resolution that enables a detailed study of the spatial structure of individual MPCs. The work offered by Santos et al. investigated outdoor responses measured with a spatial resolution of 4.8 cm and concentrated on clustered MPCs from distinct reflectors.

3.2. A Simple Multipath Extraction Algorithm

Input. The algorithm receives a matrix $\mathbf{M}_{N_x \times N_t}$ of measured impulse responses, where each row includes a single impulse response. It also receives two vectors: a vector of receiver positions $\{x_i\}_{i=1}^{N_x}$ with uniformly spaces positions and a vector of delays $\{t_j\}_{j=1}^{N_t}$ with uniformly spaced delays. In our data the spatial resolution δx varies between 2 mm and 10 mm for different measurements, and the temporal resolution $\delta \tau$ equals 28 psec.

In the following description we refer to the (i, j) position in matrices as the (x_i, t_j) position, in order to maintain the physical significance of the indices.

Two control parameters are given: a minimal spatial extent of $D_{\min}$ set to 4 cm and an amplitude threshold Thr set at 0.1 (-20 dB).

Initialization. Set to zero all points in $\mathbf{M}$ with an absolute value below a threshold set at max abs($\mathbf{M}$) $\times$ Thr. Set to zero a matrix $\mathbf{I}$ with dimensions $N_x \times N_t$ that will be used to indicate which pixels were processed.

MPC Extraction. For each location x_i for each delay t_j and if $\mathbf{I}(x_i, t_j) = 1$, that is, the (x_i, t_j) pixel in the matrix $\mathbf{M}$ was already checked, continue to the next pixel (next step of the loop). If $\mathbf{M}(x_i, t_j) = 0$, continue to the next pixel.

Set $\mathbf{I}(x_i, t_j) = 1$ to indicate that the current pixel was checked. Collect an environment of pixels around (x_i, t_j) where $\mathbf{M}$ is nonzero and has the same sign as $\mathbf{M}(x_i, t_j)$. Pixels are collected iteratively by searching over adjacent neighbors (in position or delay) for pixels already collected. For every pixel checked, set to zero the corresponding cell in the matrix $\mathbf{I}$.

After having collected a set of pixels around (x_i, t_j), approximate it by a parallelogram (over delay and receiver positions) and calculate its effective amplitude. If the resulting parallelogram extends at least $D_{\min}$ over receiver locations, save it as an estimated MPC. Otherwise reject it.

Output. A list of parallelograms over receiver position and delay, each with a signed amplitude.

4. Results

Section 4.1 compares full-band (2–17.2 GHz) measurement matrices to their reconstruction based on the multipath components extracted from them. The motivation is a comparison of two types of reconstruction, one of them incorporating multipath components with bounded areas of visibility at the receiver. Section 4.2 investigates the apparent visibility of the multipath components in responses with different carrier frequencies.

Investigation of the measured channel responses versus bandwidth, with different carriers, and bandwidth between 100 MHz and 1.5 GHz showed no significant dependence of the visibility length of MPCs on bandwidth.
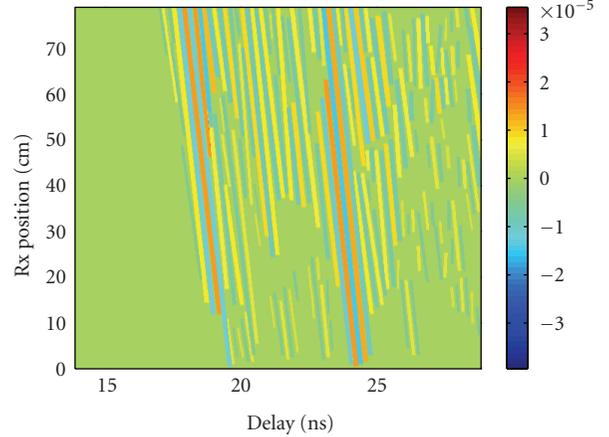

FIGURE 2: Bounded multipath components reconstruction of the measurement from Figure 1. In this reconstruction, multipath components are represented by diagonals with a fixed amplitude and a finite extent in the delay domain and in receiver locations.
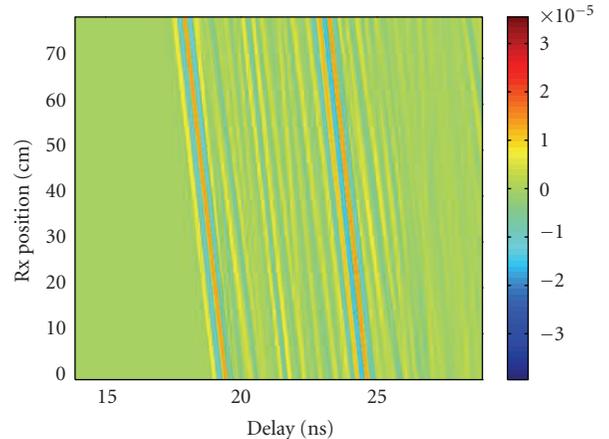

FIGURE 3: Unbounded multipath components reconstruction of the measurement from Figure 1. In this reconstruction, multipath components are represented by diagonals with a fixed amplitude that extend along the entire range of receiver locations. Note the interference between multipath components over the later delays.

4.1. Full-Band Results. We compare two types of reconstruction of measured impulse responses, both based on the multipath components extracted from them. The *Bounded* Multipath Component Reconstruction, as the example in Figure 2, is a reconstruction of a measurement matrix based on multipath components that are present over finite areas of space. The *Unbounded* Multipath Components Reconstruction, as the example in Figure 3, is a reconstruction of a measurement matrix that includes multipath components present over the *entire* range of receiver locations. The unbounded reconstruction corresponds to the classic viewpoint that attributes the spatial dynamics of the channel to the space-dependent delay of the components and to interference among multipath components that are individually stable.
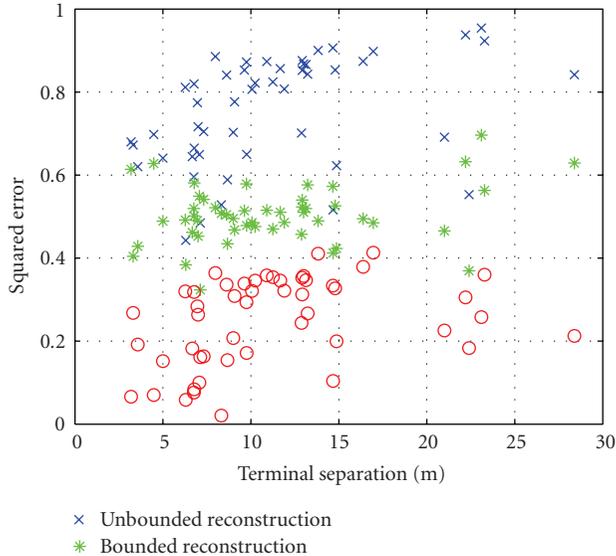
FIGURE 4: Performance of channel reconstruction based on the extracted multipath components. The exes show squared error results of the unbounded multipath components reconstruction. The stars show results of the bounded multipath components reconstruction, and the circles show the difference of squared error between the two types of reconstruction. The bounded multipath components reconstruction is superior as it achieves lower squared error.
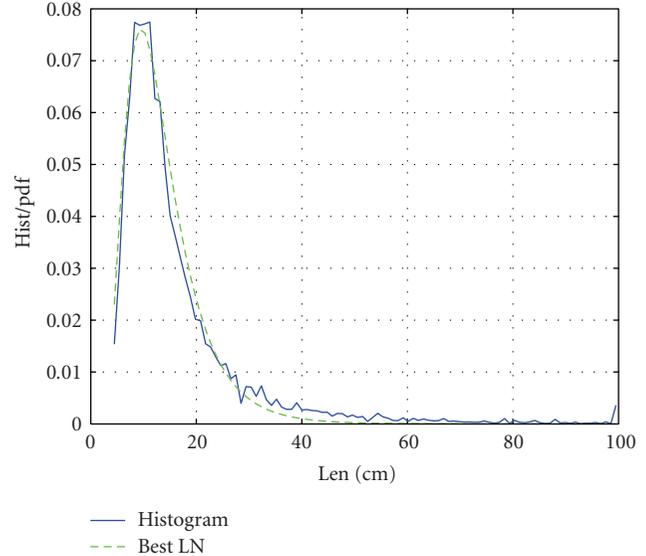

FIGURE 5: A histogram of the length of extracted MPCs that account for 80% of the channel response energy, shown with the best fit log-normal distribution, that has mean 13.6 cm and standard deviation 7.1 cm. The visibility length statistics (mean and standard deviation) over all extracted MPCs are different from the statistics averaged over individual measurements.

The amplitude of each multipath component in the unbounded reconstruction was calculated from the amplitude given by the extraction software tool using $A_{UB} = A_B(L_B/L_{UB})$, where A_B is the amplitude returned by the extraction tool (see Section 3.2), L_B is the spatial extent of the diagonal, and L_{UB} is the length of the entire receiver range, usually one meter. This choice of amplitude is best in the sense that the square error between the two types of reconstruction is minimal. v

The figure of merit we use to appreciate the two types of reconstruction is the normalized squared error (SE), that is, the squared difference between a measurement and its reconstruction, summed over receiver locations and delay values and normalized by the energy (sum of squares) of the measured data:

$$SE = \frac{\sum_{Rx\ Positions}\sum_{delay}(meas'dresponses - reconstruction)^2}{\sum_{RxPositions}\sum_{delay}(meas'dresponses)^2}. \tag{1}$$

Figure 4 presents the squared error of the entire set of measurements with the two types of reconstructions. The unbounded reconstruction is inferior to the bounded one in terms of squared error, and the difference averages (over the set of measurements) to 0.25.

The results are based on the multipath components accounting for 80% of the energy of the bounded reconstruction. We calculated the per-measurement mean and standard deviation of the length of these components, and the results, averaged over the entire set of measurements, show an average path visibility of 16.0 cm, with a standard

deviation of 26.5 cm. The average number of significant multipath components visible from each receiver location is 42.5 (We corrected the apparent number of multipath components to account for the over-sampling in the data, by multiplying the number of diagonals by 28 psec × 15.2 GHz. 28 psec is the sampling period and 15.2 GHz is the 3 dB bandwidth of the data.)

A histogram of the visibility length of the MPC extracted from all the measurements that account for 80% of the channel energy is shown in Figure 5. The log-normal distribution is a very good fit, with mean 13.6 cm and standard deviation 7.1 cm.

4.2. Subband Results:Carrier Dependence. The investigation described in this section focuses on the apparent size of the visibility areas of the multipath components, where the measured responses were filtered to different 1 GHz-wide bands. We show that the visibility areas tend to shrink as the carrier frequency increases.

The measured channel responses were filtered using a raised cosine window with 3 dBbandwidth of 1 GHz and $\beta = 0.1$. The responses measured per each receiver location along the rail were then converted to the time (delay) domain, to generate a two-dimensional representation of the channel as shown in the example in Figure 6. Figure 7 shows the measurement from Figure 6 in a different band.

An example of the average diagonal length against subband center frequency is shown in Figure 8, along with the standard deviation. This example is typical in the sense that it shows a reduction of the mean and standard deviation of the size of the visibility areas of the multipath components
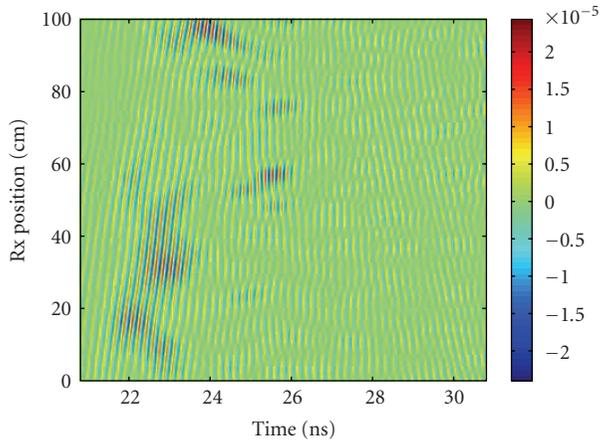
FIGURE 6: An example of measured impulse responses in the 5-6 GHz band. This example is non-line-of-sight, with terminal separation of about 6.8 meters the terminals were located at different floors of the same building. The figure shows passband impulse responses measured over a one-meter rail with receiver positions separated by 2 mm. The vertical axis represents positions along the rail, and the receiver was located closer to the transmitter at the top part of the picture than at its bottom. The carrier frequency (5.5 GHz in this case) was not removed in order to not lose the angle of arrival information, so the impulse response is real and shows a strong 5.5 GHz oscillation.
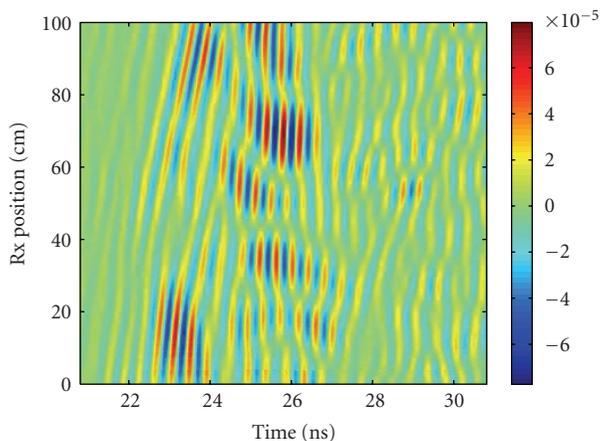

FIGURE 7: An example of measured impulse responses in the 2-3 GHz band, higher bands of the same measurement, is shown in Figure 6. Note that the diagonal features (that correspond to multipath components) are *longer* in this band than in the higher band. See comments below Figure 6.

with carrier frequency increase. The reduction of both parameters is clearer in the lower bands (2–7 GHz) over the entire set of measurements; the behavior of higher bands is less consistent.

In order to appreciate the behavior of the mean diagonal length and the standard deviation against sub-band carrier frequency, we fitted them to a linear trend. Figure 8 shows one example of a linear fit of the average length of the diagonals. All of the 50 measurements show a negative slope
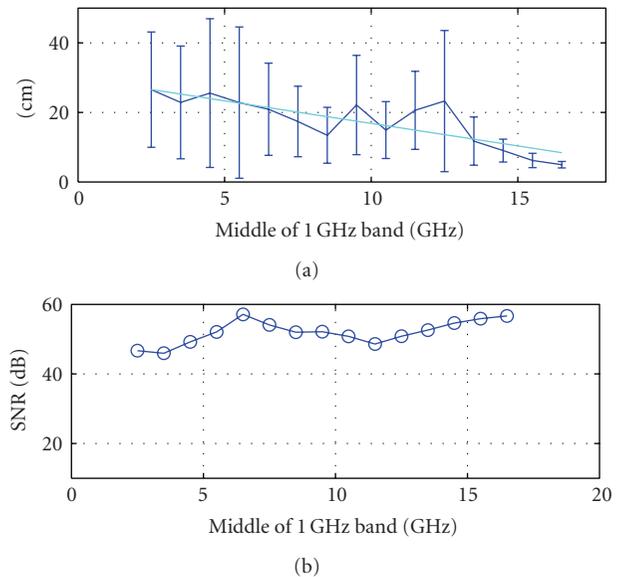

FIGURE 8: The average spatial length of multipath components accounting for 80% of the measured response energy from a single typical measurement and the standard deviation, plotted (a) against sub-band carrier frequency. The signal-to-noise ratio (SNR) is indicated (b).

of the average diagonal length and a negative slope of the standard deviation of diagonal lengths. These negative slopes indicate the reduction in the size of the visibility areas as the carrier frequency increases. More negative (steeper) slopes, which indicate a fast decrease of the size of the visibility areas, are apparent for some measurements with terminal separations below 10 meters and SNR above 40 dB.

5. Summary and Significance

This paper offers analysis of measured wideband radio channel responses, with an emphasis on the visibility of the multipath components across space. The analysis of full-band (2–17.2 GHz) measurements extracted the significant multipath components from each measurement using a simple software tool designed for this purpose and compared two simplified representations of the channel to the original measurements. The simplified measurement reconstructions were performed in two ways: (1) by considering spatially limited multipath components, i.e. paths that are seen by the receiver over limited areas in space, and (2) by considering multipath components that are seen over a fixed (one meter) range of receiver positions. The second (spatially unbounded) channel representation corresponds to the accepted philosophy of channel models, that is, the implicit assumption that multipath components are stable over a range of receiver motion. The range of receiver positions where the multipath structure is assumed to be stable is sometimes termed "small-scale" without a quantitative characterization. Our results indicate that multipath components are stable over areas of space on the order of 20–30 cm.

Line-of-sight components are more stable than nonline-of-sight ones in fact, they are seen across the entire one-meter range of our measurements. The spatial dynamics of nonline-of-sight radio channels appear to be dominated by the appearance and disappearance of multipath components.

The analysis of the responses with a bandwidth of 1 GHz showed that the size of the areas of visibility of the multipath components decreases as the carrier frequency is increased in the range of 2 GHz–17 GHz. We did not see a significant effect of the bandwidth on the visibility radius of multipath components.

This work is an initial step towards a spatially dependent channel model that will enable better design of indoor MIMO system and systems with terminal mobility. It offers a step in understanding the diffuse multipath component, a concept recently under investigation, that has been measured and characterized with lower bandwidths. Salmi et al. [43] propose to model diffuse scattering, also named diffuse multipath component (DMC), as a continuous distribution of channel response across delays, using a multivariate Gaussian variables with given correlation properties. The diffuse components of the response are understood in this model as essentially different from the specular components, that have a delta-like effect on the channel response. The spatiotemporal characteristics of the DMC are described in [44], and the work in the angular spread of the DMC is shown to be significantly correlated with the main arrivals. And the work in [44] indicates that distinguishing the DMC from "regular" arrivals is difficult.

The physical processes causing paths to appear stable over small areas also need to be investigated the connection between carrier frequency and the average size of the areas of visibility is especially interesting in this respect. A possible explanation follows the idea of "wideband Fresnel zones" suggested in [2–5, 45], defined as the area of scattering at each interaction that corresponds to the maximum carried energy from the transmitter to the receiver. Each scattering event in a path from the transmitter to the receiver is accompanied by a Fresnel zone about its center. The radius of this zone is directly related to an equivalent wavelength of the impinging wave and to the transmitter-receiver separation, and it decreases as the carrier frequency increases. The effective wavelength is estimated [4] by the mean wavelength included in the propagating waves

$$\lambda_c \sim \frac{(\lambda_{\min} + \lambda_{\max})}{2} = \frac{c}{f_c - B^2/4f_c}. \tag{2}$$

Thus, a system with a high carrier frequency experiences smaller effective scattering areas and as a result smaller areas of visibility of each multipath component.

Acknowledgments

References

[1] V. Raghavan and A. M. Sayeed, "Multi-antenna capacity of sparse multipath channels," UW ECE Technical Report 09-03, November 2009.

[2] M. Brühl, G. J. O. Vermeer, and M. Kiehn, "Fresnel zones for broadband data," *Geophysics*, vol. 61, no. 2, pp. 600–604, 1996.

[3] R. W. Knapp, "Fresnel zones in the light of broadband data," *Geophysics*, vol. 56, no. 3, pp. 354–359, 1991.

[4] J. Pearce and D. Mittleman, "Defining the Fresnel zone for broadband radiation," *Physical Review E*, vol. 66, no. 5, Article ID 056602, 4 pages, 2002.

[5] A. M. Hayar, "On the spatial and temporal degrees of freedom of UWB communications," in *Proceedings of the 12th European Wireless Conference (EW '06)*, Athens, Greece, April 2006.

[6] C. Prettie, D. Cheung, L. Rusch, and M. Ho, "Spatial correlation of UWB signals in a home environment," in *Proceedings of the IEEE Conference on Ultra Wideband Systems and Technologies*, pp. 65–69, May 2002.

[7] L. Dossi, G. Tartara, and F. Tallone, "Statistical analysis of measured impulse response functions of 2.0 GHz indoor radio channels," *IEEE Journal on Selected Areas in Communications*, vol. 14, no. 3, pp. 405–410, 1996.

[8] H. Hashemi, "Impulse response modeling of indoor radio propagation channels," *IEEE Journal on Selected Areas in Communications*, vol. 11, no. 7, pp. 967–978, 1993.

[9] J. Tsao, D. Porrat, and D. Tse, "Prediction and modeling for the time-evolving ultra-wideband channel," *IEEE Journal on Selected Topics in Signal Processing*, vol. 1, no. 3, pp. 340–356, 2007.

[10] J. W. Wallace and M. A. Jensen, "Time-varying MIMO channels: measurement, analysis, and modeling," *IEEE Transactions on Antennas and Propagation*, vol. 54, pp. 3265–3273, 2006.

[11] C. Chen and M. A. Jensen, "A stochastic model of the time-variant MIMO channel based on experimental observations," *IEEE Transactions on Vehicular Technology*, vol. 58, no. 6, pp. 2618–2625, 2009.

[12] N. Czink, T. Zemen, J.-P. Nuutinen, J. Ylitalo, and E. Bonek, "A time-variant MIMO channel model directly parametrised from measurements," *EURASIP Journal on Wireless Communications and Networking*, vol. 2009, Article ID 687238, 2009.

[13] 3GPP, "Spatial channel model for multiple input multiple output (MIMO) simulations (release 6)," Tech. Rep. TR 25.996 v6.1.0 (2003-09), 3rd Generation Partnership Project, Technical Specification Group Radio Access Network, September 2003.

[14] V. Erceg, L. Schumacher, P. Kyritsi et al., "TGn channel models," Tech. Rep. IEEE 802.11-03/940r4, IEEE P802.11 Wireless LANs, May 2004.

[15] P. Kyösti, J. Meinilä et al., "WINNER II channel models part I," Tech. Rep. IST-4-027756 WINNER II D1.1.2 V1.2, Information Society Technologies, September 2007.

[16] J. M. Kyösti, "WINNER II channel models part II," Tech. Rep. IST-4-027756 WINNER II D1.1.2 V1.0, Information Society Technologies, September 2007.

[17] M. Narandžić, C. Schneider, R. Thomä, T. Jämsä, P. Kyösti, and X. Zhao, "Comparison of SCM, SCME, and WINNER channel models," in *Proceedings of the 65th IEEE Vehicular Technology Conference (VTC '07)*, pp. 413–417, April 2007.

[18] A. F. Molisch, H. Asplund, R. Heddergott, M. Steinbauer, and T. Zwick, "The COST259 directional channel model—part I: overview and methodology," *IEEE Transactions on Wireless Communications*, vol. 5, no. 12, pp. 3421–3433, 2006.

[19] L. M. Correia, *Wireless Flexible Personalised Communications*, John Wiley & Sons, New York, NY, USA, 2001.

[20] T. Zwick, C. Fischer, and W. Wiesbeck, "A stochastic multipath channel model including path directions for indoor environments," *IEEE Journal on Selected Areas in Communications*, vol. 20, no. 6, pp. 1178–1192, 2002.

[21] C.-C. Chong, C.-M. Tan, D. I. Laurenson, S. McLaughlin, M. A. Beach, and A. R. Nix, "A novel wideband dynamic directional indoor channel model based on a Markov process," *IEEE Transactions on Wireless Communications*, vol. 4, no. 4, pp. 1539–1552, 2005.

[22] C.-C. Chong, D. Laurenson, and S. McLaughlin, "The implementation and evaluation of a novel wideband dynamic directional indoor channel model based on a markov process," in *Proceedings of the 14th IEEE International Symposium on Personal, Indoor and Mobile Radio Communications (PIMRC '03)*, vol. 1, pp. 670–674, September 2003.

[23] M. Herdin, *Non-stationary indoor MIMO radio channels*, Ph.D. dissertation, Vienna University of Technology, 2004.

[24] J. O. Nielsen, V. Afanassiev, and J. B. Andersen, "A dynamic model of the indoor channel," *Wireless Personal Communications*, vol. 19, no. 2, pp. 91–120, 2001.

[25] J. Karedal, A. J. Johansson, F. Tufvesson, and A. F. Molisch, "A measurement-based fading model for wireless personal area networks," *IEEE Transactions on Wireless Communications*, vol. 7, no. 11, pp. 4575–4585, 2008.

[26] C. Oestges, N. Czink, B. B. P. Castiglione, F. Kaltenberger, and A. Paulraj, "Experimental characterization and modeling of outdoor-toindoor and indoor-to-indoor distributed channels," *IEEE Transactions on Vehicular Technology*, vol. 59, no. 5, pp. 2253–2265, 2010.

[27] K. Hausmair, K. Witrisal, and P. Meissner, "SAGE algprithm for UWB channel paremeter estimation," in *Proceedings of the 10th COST 2100 Management Committee Meeting*, Athens, Greece, February 2010.

[28] R. J.-M. Cramer, *An evaluation of ultra-wideband propagation channels*, Ph.D. dissertation, University of Southern California, 2000.

[29] J. M. Cramer, R. A. Scholtz, and M. Z. Win, "On the analysis of UWB communication channels," in *Proceedings of the IEEE Military Communications Conference (MILCOM '99)*, vol. 2, pp. 1191–1195, November 1999.

[30] R. J.-M. Cramer, R. A. Scholtz, and M. Z. Win, "Evaluation of an ultra-wide-band propagation channel," *IEEE Transactions on Antennas and Propagation*, vol. 50, no. 5, pp. 561–570, 2002.

[31] T. C.-K. Liu, D. I. Kim, and R. G. Vaughan, "A high-resolution, multi-template deconvolution algorithm for time-domain UWB channel characterization," *Canadian Journal of Electrical and Computer Engineering*, vol. 32, no. 4, pp. 207–213, 2007.

[32] B. H. Fleury, D. Dahlhaus, R. Heddergott, and M. Tschudin, "Wideband angle of arrival estimation using the SAGE algorithm," in *Proceedings of the 4th IEEE International Symposium on Spread Spectrum Techniques and Applications*, vol. 1, pp. 79–85, September 1996.

[33] B. H. Fleury, M. Tschudin, R. Heddergott, D. Dahlhaus, and K. I. Pedersen, "Channel parameter estimation in mobile radio environments using the SAGE algorithm," *IEEE Journal on Selected Areas in Communications*, vol. 17, no. 3, pp. 434–450, 1999.

[34] C. C. Chong, D. I. Laurenson, C. M. Tan, S. McLaughlin, M. A. Beach, and A. R. Nix, "Joint detection-estimation of directional channel parameters using the 2-D frequency domain SAGE algorithm with serial interference cancellation," in *Proceedings of the International Conference on Communications (ICC '02)*, vol. 2, pp. 906–910, 2002.

[35] K. Haneda and J.-I. Takada, "An application of SAGE algorithm for uwb propagation channel estimation," in *Proceedings of the IEEE Conference on Ultra Wideband Systems and Technologies*, pp. 483–487, November 2003.

[36] M. Matthaiou and N. Razavi-Ghods, "Characterization of an indoor MIMO channel in frequency domain using the 3D-SAGE algorithm," in *Proceedings of the IEEE International Conference on Communications (ICC '07)*, pp. 5868–5872, June 2007.

[37] A. Richter, *Estimation of radio channel parameters: models and algorithms*, Ph.D. dissertation, Technische Universitt Ilmenau, Ilmenau, Germany, 2005.

[38] J. Salmi, A. Richter, and V. Koivunen, "Detection and tracking of MIMO propagation path parameters using state-space approach," *IEEE Transactions on Signal Processing*, vol. 57, no. 4, pp. 1538–1550, 2009.

[39] K. Haneda, J.-I. Takada, and T. Kobayashi, "A parametric UWB propagation channel estimation and its performance validation in an anechoic chamber," *IEEE Transactions on Microwave Theory and Techniques*, vol. 54, no. 4, pp. 1802–1811, 2006.

[40] K. Haneda, J.-I. Takada, K.-I. Takizawa, and P. Vainikainen, "Ultrawideband spatio-temporal area propagation measurements and modeling," in *Proceedings of the IEEE International Conference on Ultra-Wideband (ICUWB '09)*, pp. 326–331, September 2009.

[41] T. Santos, J. Karedal, P. Almers, F. Tufvesson, and A. F. Molisch, "Scatterer detection by successive cancellation for UWB—method and experimental verification," in *Proceedings of the IEEE Vehicular Technology Conference (VTC '08)*, pp. 445–449, May 2008.

[42] T. Santos, J. Karedal, P. Almers, F. Tufvesson, and A. F. Molisch, "Modeling the ultra-wideband outdoor channel: measurements and parameter extraction method," *IEEE Transactions on Wireless Communications*, vol. 9, no. 1, pp. 282–290, 2010.

[43] J. Salmi, J. Poutanen, K. Haneda et al., "Incorporating diffuse scattering in geometry-based stochastic MIMO channel models," in *Proceedings of the 4th European Conference on Antennas and Propagation (EuCAP '10)*, April 2010.

[44] F. Quitin, C. Oestges, F. Horlin, and P. De Doncker, "Diffuse multipath component characterization for indoor MIMO channels," in *Proceedings of the 4th European Conference on Antennas and Propagation (EuCAP '10)*, pp. 1–5, April 2010.

[45] W. Zhang, T. D. Abhayapala, and J. Zhang, "UWB spatial-frequency channel characterization," in *Proceedings of the 63rd IEEE Vehicular Technology Conference (VTC '06)*, vol. 6, pp. 2732–2736, May 2006.

EUSIPCO 2011
19th European Signal Processing Conference
August 29- September 2, 2011, Barcelona (Spain)

Photograph © Turisme de Barcelona / J. Trullàs

Preliminary call for papers

The 2011 European Signal Processing Conference (EUSIPCO-2011) is the nineteenth in a series of conferences promoted by the European Association for Signal Processing (EURASIP, www.eurasip.org). This year edition will take place in Barcelona, capital city of Catalonia (Spain), and will be jointly organized by the Centre Tecnològic de Telecomunicacions de Catalunya (CTTC) and the Universitat Politècnica de Catalunya (UPC).

EUSIPCO-2011 will focus on key aspects of signal processing theory and applications as listed below. Acceptance of submissions will be based on quality, relevance and originality. Accepted papers will be published in the EUSIPCO proceedings and presented during the conference. Paper submissions, proposals for tutorials and proposals for special sessions are invited in, but not limited to, the following areas of interest.

Areas of Interest

- Audio and electro-acoustics.
- Design, implementation, and applications of signal processing systems.
- Multimedia signal processing and coding.
- Image and multidimensional signal processing.
- Signal detection and estimation.
- Sensor array and multi-channel signal processing.
- Sensor fusion in networked systems.
- Signal processing for communications.
- Medical imaging and image analysis.
- Non-stationary, non-linear and non-Gaussian signal processing.

Submissions

Procedures to submit a paper and proposals for special sessions and tutorials will be detailed at www.eusipco2011.org. Submitted papers must be camera-ready, no more than 5 pages long, and conforming to the standard specified on the EUSIPCO 2011 web site. First authors who are registered students can participate in the best student paper competition.

Important Deadlines:

Proposals for special sessions	15 Dec 2010
Proposals for tutorials	18 Feb 2011
Electronic submission of full papers	**21 Feb 2011**
Notification of acceptance	23 May 2011
Submission of camera-ready papers	6 Jun 2011

Webpage: www.eusipco2011.org

Organizing Committee

Honorary Chair
Miguel A. Lagunas (CTTC)

General Chair
Ana I. Pérez-Neira (UPC)

General Vice-Chair
Carles Antón-Haro (CTTC)

Technical Program Chair
Xavier Mestre (CTTC)

Technical Program Co-Chairs
Javier Hernando (UPC)
Montserrat Pardàs (UPC)

Plenary Talks
Ferran Marqués (UPC)
Yonina Eldar (Technion)

Special Sessions
Ignacio Santamaría (Unversidad de Cantabria)
Mats Bengtsson (KTH)

Finances
Montserrat Nájar (UPC)

Tutorials
Daniel P. Palomar
(Hong Kong UST)
Beatrice Pesquet-Popescu (ENST)

Publicity
Stephan Pfletschinger (CTTC)
Mònica Navarro (CTTC)

Publications
Antonio Pascual (UPC)
Carles Fernández (CTTC)

Industrial Liaison & Exhibits
Angeliki Alexiou
(University of Piraeus)
Albert Sitjà (CTTC)

International Liaison
Ju Liu (Shandong University-China)
Jinhong Yuan (UNSW-Australia)
Tamas Sziranyi (SZTAKI -Hungary)
Rich Stern (CMU-USA)
Ricardo L. de Queiroz (UNB-Brazil)